

## Surface measurements of the 5 June 2013 damaging thunderstorm wind event near Pep, Texas

W. Scott Gunter<sup>\*1</sup>, John L. Schroeder<sup>1,2</sup>,  
Christopher C. Weiss<sup>1</sup> and Eric C. Bruning<sup>1</sup>

<sup>1</sup>Atmospheric Science Group, Department of Geosciences, Texas Tech University, Lubbock, Texas, USA

<sup>2</sup>National Wind Institute, Texas Tech University, Lubbock, Texas, USA

(Received January 6, 2016, Revised November 26, 2016, Accepted December 10, 2016)

**Abstract.** High-resolution wind measurements at 2.25 m in height were used to investigate the mean and turbulence properties of an extreme thunderstorm wind event in West Texas. These data were combined with single Doppler scans from the Texas Tech University Ka-band mobile Doppler radars systems (TTUKa) to provide meteorological context over the surface measurement stations for portions of the outflow. Several features characteristic of a severe wind event were noted in the radar data, including a bowing portion of the thunderstorm complex and a small circulation on the leading edge. These features were reflected in the surface wind time histories and provided natural separation between various regions of the outflow. These features also contributed to the peak 1-s gust at all measurement stations. The turbulence characteristics of each outflow region were also investigated and compared. Reduced values of running turbulence intensity and elevated values of longitudinal integral scales were noted during the period of peak wind speed. Larger scales of turbulence within the outflow were also suggested via spectral analysis.

**Keywords:** thunderstorm; non-synoptic wind and turbulence; surface measurements; radar

---

### 1. Introduction

To mitigate the lack of observed thunderstorm winds of importance to wind engineering, experimental methods are typically used to generate scaled down or numerically derived extreme thunderstorm wind time histories. These methods include physical modeling in wind tunnels and laboratories (e.g., Wood, Kwok *et al.* 2001, Letchford, Mans *et al.* 2002, Choi 2004, Lin, Orf *et al.* 2007) as well as numerical simulations of isolated downdrafts impinging on a surface (e.g., Mason *et al.* 2010, Vermeire, Orf *et al.* 2011) and full 3-D cloud models (e.g., Orf *et al.* 2012) to generate winds travelling away from a thunderstorm (outflow) at speeds relevant for design. These simulations have generally compared well with observed thunderstorm outflow winds (Kim and Hangan 2007, Lin, Orf *et al.* 2007, Orwig and Schroeder 2007). Full-scale datasets incorporating research-grade anemometry have also been beneficial in investigating the turbulence characteristics of thunderstorm winds through the application of various techniques, including block averaging, moving averages, and empirical mode decomposition (e.g., Chen and Letchford

---

\*Corresponding author, Professor, E-mail: [scott.gunter@ttu.edu](mailto:scott.gunter@ttu.edu)

2006, Orwig and Schroeder 2007, Lombardo, Smith *et al.* 2014).

Considering time varying techniques, moving averages that incorporate short averaging times (less than 60 s) have proven particularly useful in documenting thunderstorm outflow turbulence while mitigating the impacts of non-stationary features in the time history. For instance, Holmes, Hangan *et al.* (2008) found that turbulence intensity (the ratio of the 40-s standard deviation of the wind speed to the 40-s mean wind speed) was maximized along the gust front, while the time period containing the maximum mean wind speed exhibited lower values of turbulence intensity. In a study of multiple thunderstorm outflow events, Lombardo, Smith *et al.* (2014) found that outflow turbulence parameters (including turbulence intensity and gust factor) were within the bounds of those computed from stationary non-convective winds for averaging times between 15 and 60 s.

To address the continuing need for high-resolution thunderstorm wind measurements, Texas Tech University (TTU) designed a field study to specifically target data collection in extreme thunderstorm winds with two mobile Doppler radars and a fleet of portable, rapidly deployable, surface meteorological stations. This study uses these combined measurements to provide an overview of a damaging, thunderstorm outflow wind event that impacted Lubbock, Texas, and the surrounding region on 5 June 2013. After a description of the structure of the thunderstorm complex driving the high winds, the turbulence characteristics of the winds associated with this event will be investigated and compared to the results of previous studies.

## 2. Data collection

### 2.1 TTU instrumentation

Surface measurements were collected with the TTU-designed StickNet fleet (Weiss and Schroeder 2008). This portable network of 24 small weather stations can be rapidly deployed in the path of severe thunderstorms (or hurricanes) and has been designed to withstand harsh environments while taking quality measurements. Each station is equipped with instrumentation to measure standard atmospheric variables (including wind speed and direction) at approximately 2.25 m above ground level (AGL). Deploying an array of StickNet towers in the path of a severe thunderstorm is often complicated by short lead times as well as road network limitations. Additionally, StickNet tower retrievals often occur after sunset. While these factors typically prohibit an in depth visual assessment of site roughness characteristics, great care is taken to avoid large obstacles upon deployment and to note features that may enhance turbulence at a particular tower location. Both single-Doppler and dual-Doppler data from the TTUKa mobile Doppler radars were also available during this event. An overview of the radar systems and data collection strategies is given in Gunter and Schroeder (2015).

### 2.2 StickNet anemometry and instrument response

The StickNet fleet of 24 deployable towers has undergone several upgrades since its inception in 2008. Most notably, these upgrades include transitioning 12 towers that employed a sonic wind sensor (Skinner, Weiss *et al.* 2011), to the more ruggedized RM Young 05103V Wind Monitors, which are capable of measuring wind speeds up to  $100 \text{ m s}^{-1}$  at a sampling interval of 10-Hz. All towers deployed for the event studied herein employed the propeller-vane Wind Monitors, but five

of the deployed towers collected data at 5-Hz. The inertia associated with these wind sensors mechanically filters the wind, not unlike a low-pass filter. The degree to which the measurements are filtered depends on the distance constant, which is 2.7 m for the propeller. Relating the distance constant to the performance of the anemometers through a first-order linear differential equation (Brock and Richardson 2001, Schroeder and Smith 2003), the magnitude of a gust with a 30 m wavelength will be reduced by 13% of its true value. Additionally, the second-order response characteristics of the vane act to increase the variance of the lateral wind speeds as well as the magnitudes of lateral turbulence intensity and certain regions of the lateral spectra (Schroeder and Smith 2003). For the 05103V Wind Monitors, with a 7.4 m damped natural wavelength, this addition of energy occurs between 0.4 and 5.4 Hz for the range of wind speeds observed in this study (3-40 m s<sup>-1</sup>). This information is useful for characterizing the likely magnitude of errors in subsequent analyses. Quality control steps did not seek to correct for these effects.

### *2.3 Data quality control*

StickNet data records were initially inspected for completeness, data spikes and/or drops due to instrument malfunction, and instrument biases. Once identified, suspicious data points were removed from the record. While the data quality varied slightly between individual platforms, quality control methods only removed 0.8% of all StickNet data points. The presence of instrument biases was investigated by comparing data from adjacent probes during the uniform inflow conditions prior to passage of the gust front in this event. 5-min mean values of both state and kinematic variables from each probe were examined and outliers were flagged for bias correction. As there were substantial differences across the relatively short extent of the array, data from the West Texas Mesonet (WTM; Schroeder, Burgett *et al.* 2005) were used to improve the bias corrections (for all variables except wind speed). The closest WTM station was located 15.8 km to west of the StickNet array, near the town of Morton, Texas. A 15-min period of pre-outflow conditions in the WTM and StickNet data was selected for wind speed and direction comparisons. Despite the approximately 8 m difference in measurement height, the difference in the mean wind direction at the Morton WTM station and StickNet 102 over the selected time period was only 3.75°. Thus StickNet 102 was used to correct wind direction biases throughout the array. State variables were corrected based on the 15-minute mean values from the Morton WTM station. Temperature and relative humidity only exhibited slight biases when compared to 1.5 m values of the WTM station. To correct StickNet barometric pressure, WTM barometric pressure was hydrostatically reduced to the mean elevation across the StickNet array (elevation across the array only varied by approximately 5 m) before comparison and subsequent adjustment. Instrument biases based on the above procedure are included in Table 1. Of the eleven towers deployed, eight recorded the event in its entirety. However, ten towers collected quality data through the peak of the event and were considered for analysis. The sampling rate varied between the ten towers, with some towers collecting at 10-Hz and others at 5-Hz. To facilitate a uniform analysis, data from the 10-Hz towers were reduced to 5-Hz by selecting every other observation within the 10-Hz records.

### *2.4 The 5 June 2013 TTU deployment*

TTU teams deployed in northwestern Hockley County near the small community of Pep, Texas approximately 45 min prior to the arrival of the gust front. This area was selected primarily for the large extent of generally flat terrain as well as a viable road network. To facilitate dual-Doppler

data collection over StickNet, the array of towers was arranged along an east-west road, while TTUKa1 was deployed to the southeast of the array on SR 303 and TTUKa2 deployed northeast of the array on SR 597 (Fig. 1). Through the collection period, the TTUKa Doppler radars employed vertical range-height indicator (RHI) scans to acquire dual-Doppler profiles and horizontal plan position indicator (PPI) scans to document the horizontal structure of the outflow. The coordinated RHI scans were conducted such that the intersection of the RHI planes (and thus the dual-Doppler profile location) was close to the first tower in the StickNet array (Fig. 2). The StickNet array itself was composed of two parts: a finescale array on the eastern end that incorporated small spacing between towers and a coarse array on the western end where a larger tower spacing was used for the purpose of capturing various sizes of length scales. Using this construction, 10 towers were deployed over a total distance of 1.27 km (Fig. 2). Elevation varied only slightly across the StickNet array with a maximum difference of 5 m, such that Tower 111 was the highest at 1117 m above mean sea level (AMSL) and Tower 107 was the lowest at 1112 m AMSL. Considering inflow conditions (with an array-wide mean wind direction of  $86.4^\circ$ ), recently plowed fields on either side of the road resulted in few obstructions for most towers. However, StickNet platforms on the eastern end of the array were likely impacted by a house and some small obstructions within 100 m of the first tower along the azimuth of the mean inflow wind speeds. Within the outflow (with winds generally from  $300^\circ$ ), few obstructions existed upstream of the western end of the array. Low scrub, a few small bushes, and a slight depression likely contributed to increased turbulence in the outflow for the eastern four StickNet platforms (106, 104, 103 and 102). Stull (1988) indicates this type of terrain (level plains with few trees or obstructions) reflects aerodynamic roughness ( $z_o$ ) lengths between 0.01 and 0.006 m. The Davenport classification scheme, employed by ASCE 7-10, is similar with values between 0.03 - 0.005 m for the open and smooth categories, respectively (ASCE 2010).

Table 1 Instrument Biases for 5 June 2013 StickNet deployment. Variables include wind direction (WD), temperature (Temp), relative humidity (RH) and barometric pressure (BP). Positive WD biases indicated clockwise correction, while negative biases indicated counter-clockwise correction

Tower	WD ( $^\circ$ )	Temp ( $^\circ\text{C}$ )	RH (%)	BP (hPa)
102	0.00	1.17	-3.48	-5.73
103	9.94	0.83	-3.80	1.59
104	-29.11	2.44	-5.43	-2.50
105	-29.83	1.79	-4.68	-2.31
106	-15.46	3.20	-4.00	0.15
107	-21.71	3.04	-2.61	0.05
108	30.48	3.97	-2.69	-2.23
109	-57.82	0.14	-4.90	-8.07
111	-21.04	3.57	-0.28	0.40
112	-40.49	2.86	-1.81	1.79

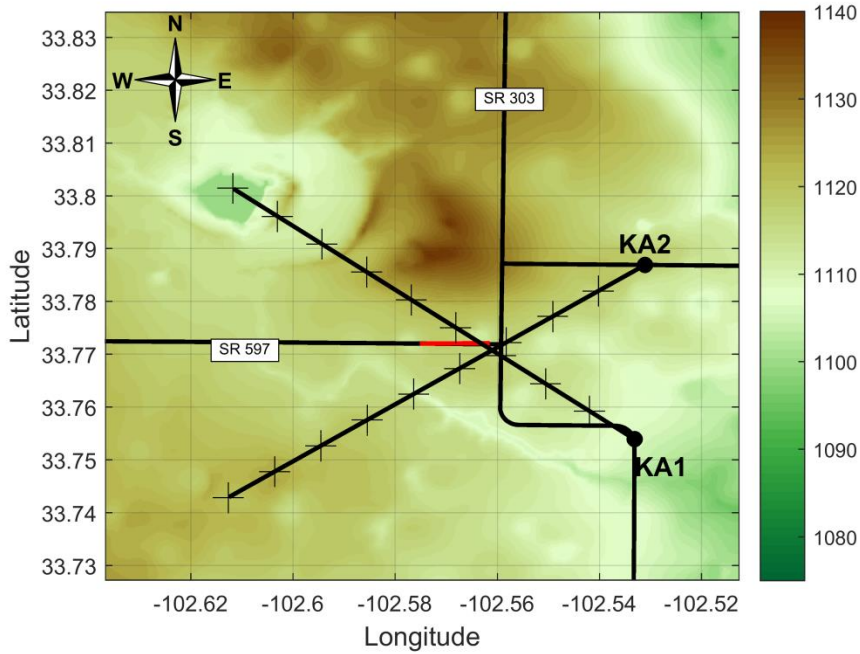


Fig. 1 Map of the 5 June 2013 TTU deployment location just south of Pep, Texas. Elevation above sea level (m) is indicated by the shading. The white line along SR 597 represents the length of the StickNet array. TTUKa radar locations are indicated by the black dots with each radar labeled. The black lines with '+' symbols describe the north-relative azimuth of each radar, while the '+' represent 1 km along the azimuth

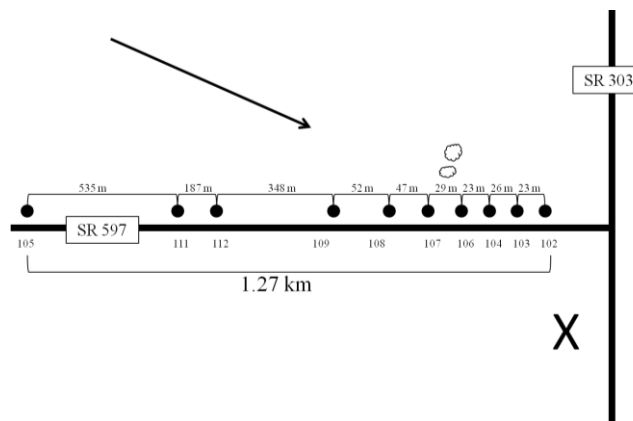


Fig. 2 A zoomed in schematic of the StickNet array (not to scale). Each tower is represented by a black dot and is labeled below the road. The distance between each probe is listed above the bracket. The approximate locations of substantial roughness elements are described by the scalloped black circles north of Towers 106 and 107, while the approximate location of the dual-Doppler wind profile location is indicated by the 'x'. The primary direction of the outflow winds is indicated by the black arrow

### 3. Event overview

The extreme surface wind speeds measured by the TTU platforms and documented herein originated from a large complex of thunderstorms that travelled southeast out of eastern New Mexico on the evening of 5 June 2013. Prior to entering the deployment domain of the TTU measurement systems, storm characteristics were documented by the Weather and Surveillance Radar (WSR-88D) operated by the National Weather Service and the WTM 10 m tall measurement stations. As seen in Fig. 3(a), the leading edge of the outflow (the gust front) initially appeared as a thin line of reflectivity stretching from southwest to northeast through Bailey County. Behind the outflow boundary, much higher reflectivity values indicated heavy rain and hail associated with the main downdraft of the storm. Additionally, the WTM station in northeastern Bailey County measured a peak 3-s gust of  $22 \text{ m s}^{-1}$  just prior to the onset of the heavy precipitation (Fig. 3(a)).

Approximately 30 minutes later, the gust front stretched from northern Yoakum County, through Hockley and Lamb counties (Fig. 3(b)). In addition to higher values of reflectivity evident behind the gust front, a bulge formed along the gust front in northern Hockley County. Such bulging features often signify the presence of a vertically-oriented circulation along the gust front as well the formation of strong surface winds (Fujita 1978). Indeed, the WTM station in Morton, Texas (northeastern Cochran County) measured a 3-s gust of  $32 \text{ m s}^{-1}$  during this period. WSR-88D radial velocity data from this period also indicated the presence of the vertical circulation (not shown). Ahead of the gust front, 5-min mean wind speeds at 10 m AGL were between 9 and  $12 \text{ m s}^{-1}$  out of the east-northeast near Lubbock, Texas. The red box in northwestern Hockley County (Fig. 3) defines the deployment domain (see Fig. 1 and 2) of the TTU measurement systems.

As the complex entered western Lubbock County 30 minutes later, the bulge persisted as new cells developed along the outflow to the south (Fig. 3(c)). A notch of reduced reflectivity to the rear of the bulge suggests the presence of a rear inflow jet and the transition to a bow echo configuration, as in Fujita (1978). Along the northern edge of this feature, the Reese Center WTM station (west-central Lubbock County) measured a 3-s gust of approximately  $34 \text{ m s}^{-1}$ . While the 5-min averaged wind direction was generally northwest behind the gust front (as indicated by the wind barbs in Figs. 3(a)-3(c)) for most stations, the 5-min average wind direction at Reese Center was westerly. This difference was mostly likely due to the falling pressures associated with the circulation and subsequent response of the surface wind field to the pressure gradient.

The bowing portion of the thunderstorm complex passed through the southern part of the city of Lubbock approximately 30 minutes later where a 3-s gust of almost  $29 \text{ m s}^{-1}$  measured at the Lubbock WTM station (Fig. 3(d)). Damage to structures as well as downed trees and power lines were reported. Wind speeds well behind the gust front remained relatively high as evidenced by the 3-s gust reported by the Reese (exceeding  $30 \text{ m s}^{-1}$ ) and Morton (exceeding  $28 \text{ m s}^{-1}$ ) WTM stations. 5-min mean wind speeds at these stations were also elevated with values of 25 and  $20 \text{ m s}^{-1}$  respectively. This thunderstorm complex progressed eastward through the remainder of the evening with continued reports of high wind and wind damage (SPC 2013; NWS 2013).

The availability of single Doppler horizontal radar scans allows for the identification of specific storm features within the small area of the TTU deployment domain at much greater resolutions. The horizontal scans of reflectivity and radial velocity from TTUKa2 were edited to remove erroneous data (including stationary ground targets) and objectively analyzed to a Cartesian grid at 60 m AGL, centered on the deployment domain. While multiple scans were collected, only reflectivity and radial velocity data at 02:30:10 UTC are shown in Fig. 4. These data correspond to the time period of Fig. 3(b) as well as the time period close to the peak wind speed measured along

the eastern end of the StickNet array. Radar reflectivity data qualitatively show a counter-clockwise “curl,” indicative of a circulating wind field, not dissimilar from the classic “hook echo” of supercell thunderstorms (Fig. 4(a)). This is further examined in Fig. 4(b) where the radial velocity data display a “couplet”, or juxtaposed inbound and outbound radial velocities that indicate a broad counter-clockwise vertical circulation in the wind field. Given the size of the feature, approximately 2 km in horizontal diameter (at 60 m AGL), it can most likely be classified as a misovortex (Fujita 1981). Similar vertically oriented circulations along thunderstorm gust fronts have been shown to enhance wind speeds in the region around the circulation (Wakimoto, Murphey *et al.* 2006). The influence of the misovortex (used interchangeably with “circulation”) on the surface wind field will be investigated further in the next section. Also evident in Fig. 4(b) are the faster winds in the main body of the outflow with inbound radial velocities in excess of  $30 \text{ m s}^{-1}$ .

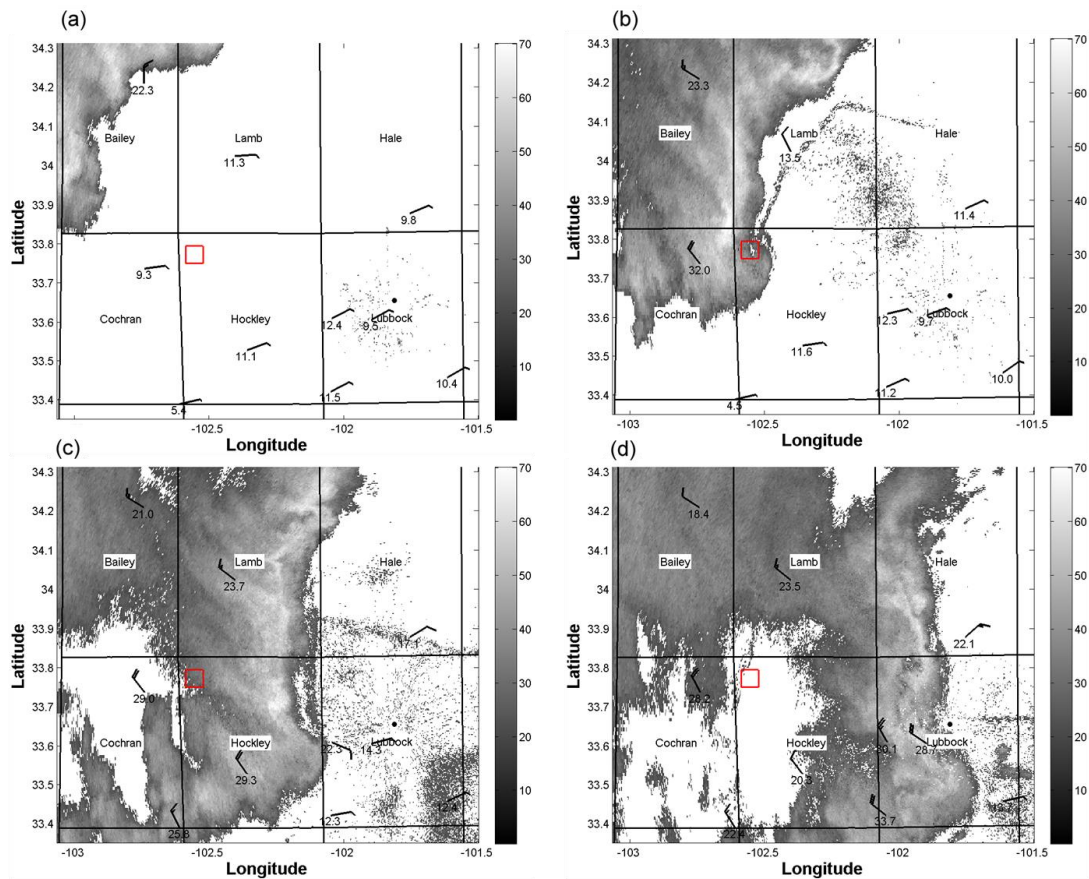


Fig. 3 Reflectivity (dBZ) from the WSR-88D in Lubbock, Texas (shading), with wind barbs from selected WTM stations For (a) 02:03:54 UTC, (b) 02:29:30 UTC, (c) 02:55:04 UTC and (d) 03:12:07. The wind barbs are the 5-min mean wind speed and direction. Longer hash marks are  $10 \text{ m s}^{-1}$ , while shorter hash marks are  $5 \text{ m s}^{-1}$ . The value below the barb is the peak 3-sec gust recorded at 10 m for the 5-min period closest to the radar volume time. The red square outlines the TTU deployment location. County boundaries and names are given and referred to in the text

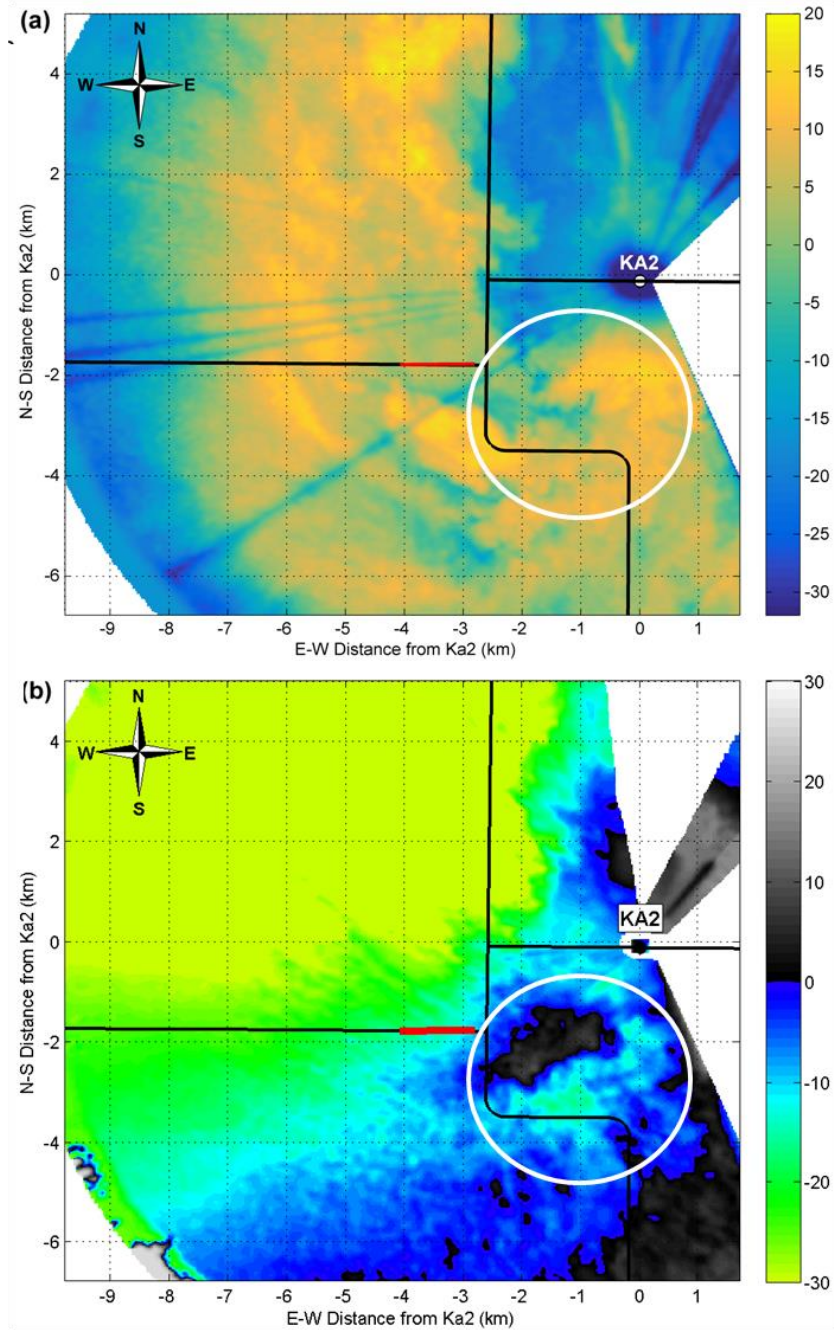


Fig. 4 TTUKa2 Reflectivity (a) and Radial Velocity (b) from 02:30:10 UTC. Values of reflectivity are in dBZ and values of radial velocity are in  $\text{m s}^{-1}$ . Negative radial velocities are radially inbound toward the radar, while positive radial velocities are radially outbound from the radar. Features highlighted include the location of the StickNet Array (horizontal red line) and the circulation discussed in the text (white circle)

#### 4. General outflow structure

While the WSR-88D and WTM provided a broad perspective of the event as it transpired across West Texas, the TTUKa radars and StickNet array similarly provided a complementary higher-resolution, local perspective of the small region of the thunderstorm complex that passed through the deployment domain. The particular region of the outflow was unique in that it included the effects of the misoscale circulation (Fig. 3(b)) in addition to the features typically observed in thunderstorm outflows (gust front, wind ramp, etc.).

##### 4.1 StickNet 102 mean time histories

To highlight the StickNet representation of the structural features observed in the TTUKa2 radar data, a centered moving average window was applied to the wind direction and speed time history of StickNet 102. The use of such a window allows for the generation of a running mean wind direction and speed thus separating the deterministic storm-scale features from turbulent fluctuations (Holmes, Hangan *et al.* 2008, Lomabrdo, Smith *et al.* 2014). Upon separation, the mean of the residual turbulence should be near zero. Larger mean residual turbulence values indicate contributions from the deterministic component. As in previous studies, multiple averaging times were investigated to examine the behavior of the mean residual turbulence. The values in Fig. 5 echo previous observations in that the 2.25 m mean residual turbulence begins to diverge from zero with larger averaging times. Considering these results and to maintain consistency with previous work, an averaging window 40-s in length was used (Holmes, Hangan *et al.* 2008).

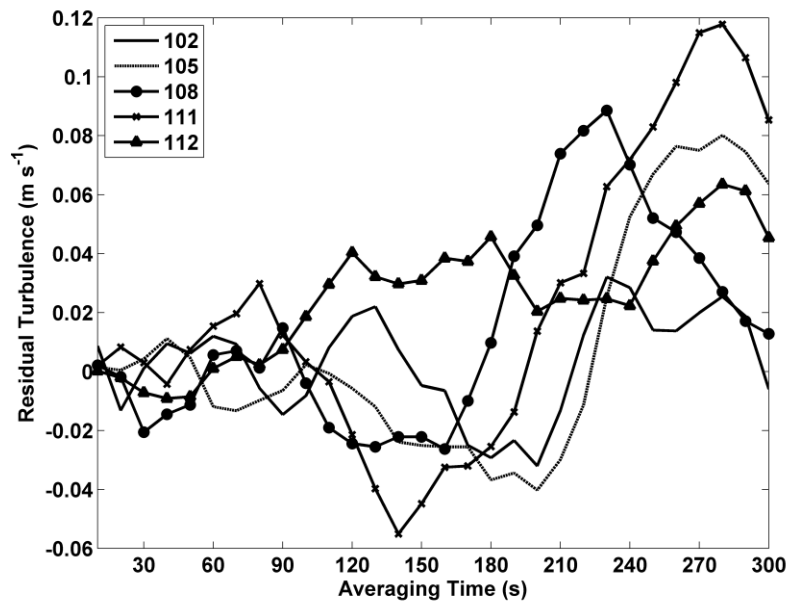


Fig. 5 Variation of the mean residual turbulence with averaging time for all StickNet towers

Several features were evident in the 40-s running mean wind direction time history: the inflow, the primary gust front (GF), an intermediate region of the outflow (R1), a secondary surge (GF2), and the main body/core of the outflow (R2; Fig. 6(a)). To further examine these features, the mean wind direction time history was segregated by the zero-derivative points on either side of the sharp changes in the 40-s mean wind direction curve seen in Fig. 6a. This methodology follows from the traditional kinematic definition of gust fronts and surges embedded in the outflow (Goff 1976, Wakimoto 1982). Segregation of the different outflow regions by wind direction has the added benefit of isolating the effects of surface roughness, which is directionally dependent. The inflow and the GF regions of the mean wind time histories reflect expectations that the GF acted as a transition zone between the inflow and outflow with the wind direction veering from  $\sim 93.5^\circ$  to  $\sim 241^\circ$  as demonstrated by Tower 102 (Fig. 6(a)). Further, a minimum in wind speed was also evident in the GF region (Fig. 6(b)) as a result of stagnation at the gust front (Wakimoto 1982). Region 1 (R1) comprises the time period after the passage of the gust front and prior to the influence of circulation. Wind direction during this period was relatively stable, while the 40-s mean wind speed initially increased to over  $15 \text{ m s}^{-1}$ . The circulation passed slightly north of the StickNet array during the GF2 region, which coincides with Figs. 4(a) and 4(b). The effect of the eastward propagation of the circulation was to veer the winds and increase the 40-s mean wind speed to near  $25 \text{ m s}^{-1}$ . Similar circulations along gust fronts have been shown to generate higher winds on their southern flank due to the superposition of the storm motion and the circulation wind vectors (Wakimoto, Murphey *et al.* 2006). The main core of the outflow corresponds to region 2 (R2), where the mean wind direction stabilizes around  $300^\circ$  and the 40-s mean wind speed reaches a peak of  $27.2 \text{ m s}^{-1}$ .

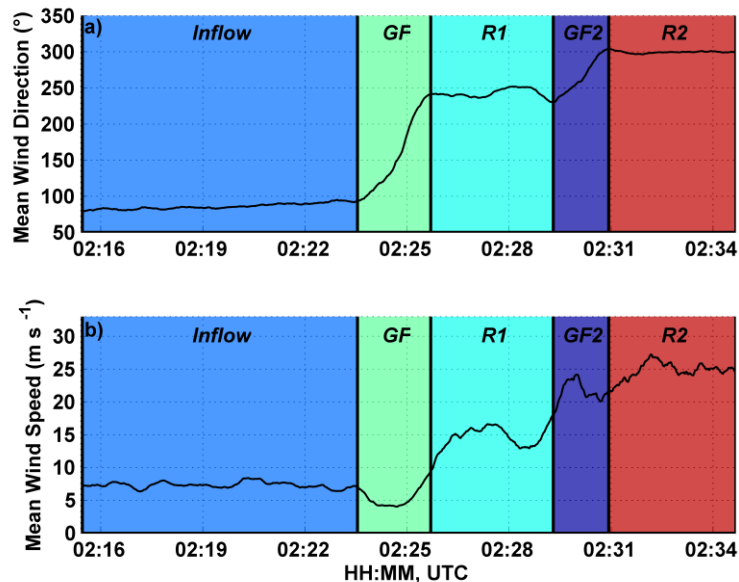


Fig. 6 Time histories of the 40-s mean wind direction (a) and speed (b) from StickNet Tower 102. The regions of the outflow discussed in the text are shaded

### 4.2 Gust characteristics

The peak gusts measured during this event demonstrate the structure of the outflow and the effects of nearby roughness elements. Gust wind speeds were computed for each tower by averaging 1 s of 5-Hz data in a moving window. The 1-s averaging window was chosen based on the recommendations of Kwon and Kareem (2014) as well as to facilitate comparisons with previous results (Holmes, Hangan *et al.* 2008, Lombardo, Smith *et al.* 2014). There was substantial variability in the peak 1-s gust magnitude and direction over the extent of the array (Fig. 7(a)) with a 15.1% difference between the largest and smallest peak 1-s gust. However, all peak 1-s gusts were measured in either the GF2 region (in association with the circulation) or the R2 region (in association with the main body of the outflow). The peak 1-s gusts measured in the GF2 region were generally similar between all towers and had more of a southwesterly component, while the peak 1-s gusts measured in the main body of the outflow appeared greater in magnitude and from the northwest. However, several towers (102, 103, 104, and 106) were downstream of roughness elements along the azimuth of the R2 wind direction, which likely reduced the impact of the gusts in the main body of the outflow.

Non-local gust factors were defined as in Holmes, Hangan *et al.* (2008) and Lombardo, Smith *et al.* (2014) as the ratio between the peak 1-s gust occurring anywhere in the time history and the largest 40-s running mean wind speed found in the time history (non-local)

$$NGF = \frac{\bar{U}_1}{\bar{U}_{40}} \tag{1}$$

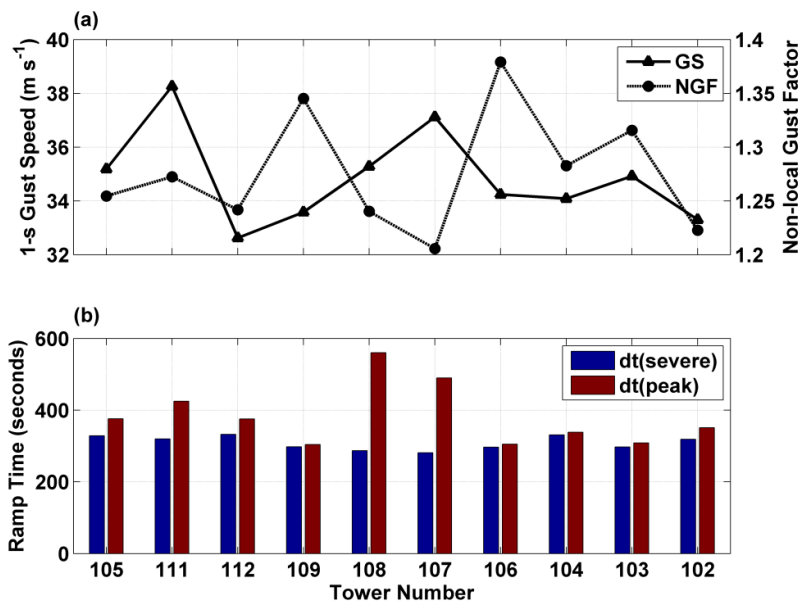


Fig. 7 Spatial distribution of the (a) peak 1-s gust (GS) and non-local gust factor (NGF) and (b) the ramp times, where dt(severe) ramp time to the severe threshold and dt(peak) is the ramp time to the peak 1-s gust

Based on this definition, non-local gust factors in Fig. 7(a) ranged from 1.21 (Tower 107) to 1.38 (Tower 106). Though the definitions are similar, the wind speed data analyzed in Holmes *et al.* (2008) were collected at 10 m AGL over similar terrain and thus gust factor values were lower than the values computed herein. Lombardo, Smith *et al.* (2014) similarly analyzed data from a StickNet tower in a supercell thunderstorm. Using a running mean of 34 s, the non-local gust factor computed for the StickNet data was similar to the values reported herein. Eq. (8) of Lombardo, Smith *et al.* (2014) was used to account for the difference in averaging time and resulted in a value of 1.29, which was close to the array mean of 1.28 for the current study.

The peak ramp time, defined as the time in seconds between the minimum at the gust front and the peak 1-s gust, varied depending on whether the peak gust occurred in association with the main body of the outflow or was measured in the GF2 region. Regardless, peak ramp times were greater than 5 min for all towers with a minimum peak ramp time of 304 s and a maximum of 560 s. Although the measurement height was only 2.25 m, most towers eclipsed the threshold of severe wind, defined by the United States National Weather Service as  $26 \text{ m s}^{-1}$ , 330 s after the gust front (Fig. 7(b)). These time scales are similar to those documented in Orwig and Schroeder (2007) for a derecho-producing MCS and the bow echo discussed in Lombardo, Smith *et al.* (2014). These similarities suggest that peak wind speeds may be found well behind the gust front in organized, quasi-linear convection.

## 5. Outflow turbulence characteristics

Previous studies have focused on comparing extreme thunderstorm winds to those characteristic of synoptically driven boundary layers as well as determining appropriate averaging times and methods by which to extract turbulence from nonstationary thunderstorm wind records (e.g., Choi and Hidayat 2002, Orwig and Schroeder 2007, Lombardo, Smith *et al.* 2014). Given the temporary nature of the StickNet deployment, a comprehensive assessment of the synoptic winds at the deployment site is unavailable. However, most towers were deployed with enough lead-time to sufficiently sample the storm inflow environment. While this environment may not be entirely representative of synoptically driven flow, it still provides a point of comparison with which to investigate the turbulence characteristics of the outflow winds. Longitudinal and lateral wind speeds were determined by computing the mean wind direction of each 40 sec segment. Within each segment, the mean wind direction was subtracted from the observed wind direction. The longitudinal wind speed was then computed as the cosine of that angle and the lateral wind speed was computed as the sine of that angle. Residual turbulence was then computed by subtracting the 40-s running mean longitudinal wind speed from the original longitudinal wind speed time histories (Holmes, Hangan *et al.* 2008, Lombardo, Smith *et al.* 2014). Short duration averaging windows have been shown to minimize the mean of the residual turbulence as well as limit the effects of nonstationarities without modifying the wind speed record (i.e., trend removal; Holmes, Hangan *et al.* 2008, Orwig 2010).

### 5.1 Turbulence intensity

Longitudinal turbulence intensity was computed by dividing the longitudinal root-mean square (RMS) turbulence time history by the 40-s running mean longitudinal wind speed time history

$$I_u = \frac{\sqrt{\overline{(u')^2}}}{\bar{U}_{40}} \quad (2)$$

where

$$u' = U - \bar{U}_{40} \quad (3)$$

The time histories of the longitudinal wind speed and  $I_u$  for Tower 111 are given in Fig. 8. The five regions of the time history, defined previously, are also indicated. The 2.25 m  $I_u$  values for the inflow varied between 6 and 18.6%, began increasing several minutes prior to the passage of the gust front, and reached a maximum of 35% within the GF region. Despite using a short averaging window, this peak is likely associated with the non-stationary ramp in wind speed near the end of the gust front segment. Turbulence intensity values remained above 10% through most of R1 before increasing slightly in the GF2 region. Shortly after the passage of the circulation associated with the GF2 region,  $I_u$  dropped to levels comparable to the inflow as the wind speeds increased to over  $30 \text{ m s}^{-1}$ . The drop in  $I_u$  associated with the peak wind speeds is consistent with the analysis of a supercell RFD in Holmes, Hangan *et al.* (2008), where 10 m  $I_u$  values decreased to 9-11% as wind speeds increased to over  $25 \text{ m s}^{-1}$ .

Fig. 8 is generally representative of the  $I_u$  time histories computed for all towers, but there was variation along the array attributable to both storm scale features and local roughness elements. The mean turbulence intensity values were computed for each region of the time histories and are displayed in Fig. 9(a) as the towers were deployed west (Tower 105) to east (Tower 102).

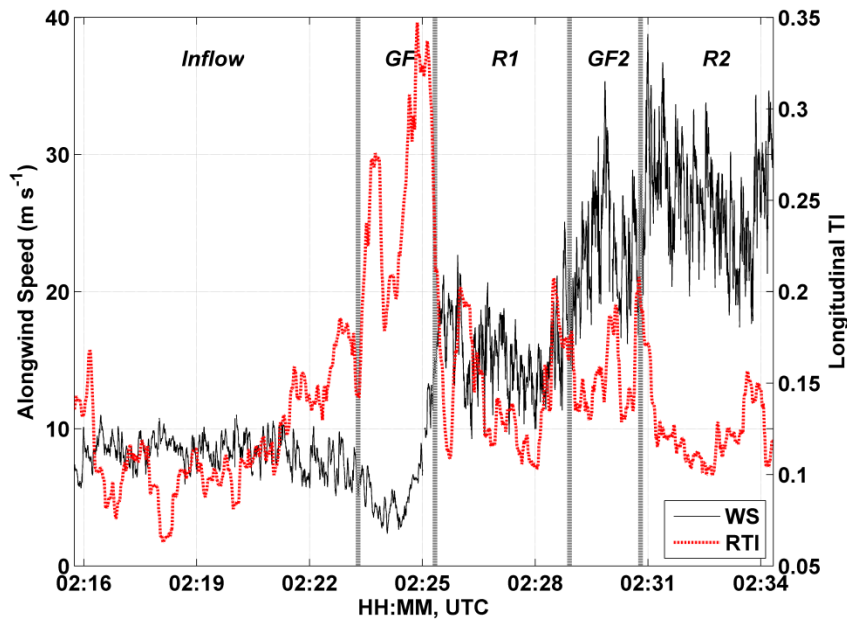


Fig. 8 Time history of the along wind (longitudinal) wind speed and running turbulence intensity (RTI) from StickNet Tower 111

In Fig. 9(a), it is evident that most towers experienced the greatest turbulence intensity in the GF region. The non-stationary ramp in the wind speeds after the wind speed minimum mostly likely contributed to the high mean values of  $I_u$  (between 16 and 25%) within this region. During the time period of maximum instantaneous wind speeds (R2 for most towers), the mean longitudinal turbulence intensity was similar in magnitude to the values computed for the inflow region with mean values just above 10%. Considering only the time periods when the 40-s mean wind speed exceeded  $25 \text{ m s}^{-1}$  (Holmes, Hangan *et al.* 2008), the mean  $I_u$  for all towers was 12.5%. Included in this value were the eastern three towers (102, 103, and 104), which most likely experience enhanced turbulence due to a small patch of brush immediately upstream of towers 102-104 for the wind directions associated with the GF2 and R2 outflow regions. Excluding these towers, the mean  $I_u$  for the same period is reduced to 11.2%. The largest mean turbulence intensity values for towers 103 and 104 were determined to be in GF2 region (as compared to the GF region for the other towers). Similarly, most towers experienced the lowest lateral turbulence intensity ( $I_v$ ; computed as in Eq. (3), but with lateral RMS turbulence) in the inflow or R2 region (Fig. 9(b)) likely owing to the more stable wind directions during these time periods. Otherwise, the gust front regions (GF and GF2) had the largest mean  $I_v$ , with values between 15 and 20% for most towers. Despite significant quality control, noise in the wind direction data of Tower 104 inflated the lateral turbulence intensities. Turbulence intensity ratios ( $I_v/I_u$ ) displayed no consistent trend between the different regions (Fig. 9(c)). However, the magnitudes were higher than those measured in neutrally stratified layers (0.67) at 11 m AGL (Counihan 1975, Teunissen 1980). A similar overestimation has been observed in the hurricane boundary layer (Schroeder and Smith 2003).

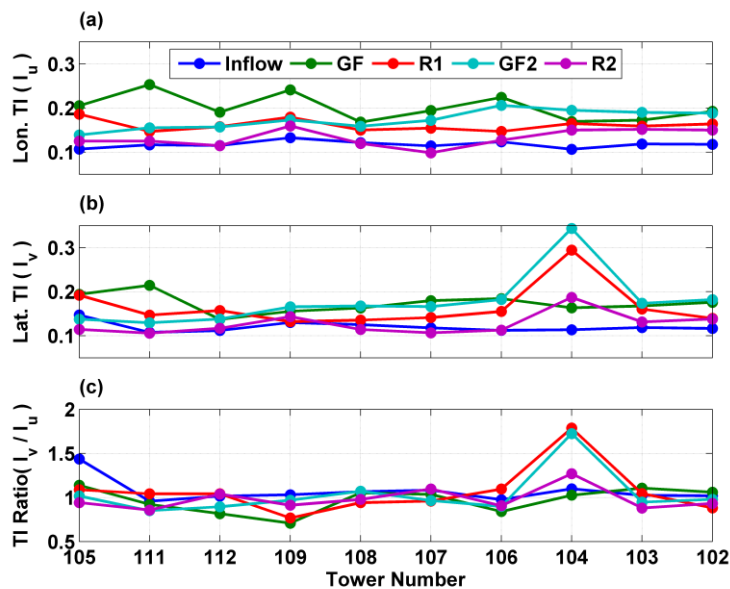


Fig. 9 Spatial distribution of mean turbulence intensity for each outflow region along the StickNet array for the (a) longitudinal turbulence intensity, (b) the lateral turbulence intensity and (c) the ratio of lateral to longitudinal turbulence intensity. The towers are arranged west (left) to east (right)

## 5.2 Integral scales

For each tower in the array, the longitudinal integral scale, or the estimated mean gust size in the longitudinal dimension, was computed by performing an exponential fit to the autocorrelation function of a 40-s segment of residual turbulence ( $u'$ ). The fit was truncated where the derivative equaled zero and then integrated to infinity (Schroeder and Smith 2003). The resulting time scale was multiplied by the mean wind speed of the segment to estimate the integral length scale

$$L_u^x = \bar{U} \int_0^\infty \rho_{uu}(\tau) d\tau \quad (4)$$

where  $L_u^x$  represents the length scale of the longitudinal wind component,  $\bar{U}$  represents the 40-s mean longitudinal wind speed, and  $\rho_{uu}(\tau)$  is the autocorrelation coefficient for time lag ( $\tau$ ). A 50% segment overlap was used, and each segment was assumed to be independent and stationary (Schroeder and Smith 2003). Further, the integral scale time history was divided into the previously defined regions as was done with turbulence intensity.

As seen from the perspective of Tower 111, the length scales of the inflow were generally less than those of the outflow (Fig. 10). Integral scales increased quickly in association with the gust front, but mean wind speeds during these periods were relatively low ( $\sim 10 \text{ m s}^{-1}$ ). The peak  $L_u^x$  for Tower 111 occurred in the GF2 region where the estimated mean gust size exceeded 100 m, before decreasing again in R2 as the peak wind speeds of the event were experienced. The latter observation suggests that larger scales of turbulence were active in the outflow, particularly GF2 and R2, as compared to the inflow. The trends noted in the data of Tower 111 were fairly consistent across the array (Fig. 11). The mean  $L_u^x$  values were uniformly smaller in inflow as compared to other regions of the outflow for all towers. Values ranged from 15 to 24 m in the inflow to between 31 and 46 m in R2 of the outflow, representing a near 50% increase. Some of this increase is most likely attributable to larger mean wind speeds within the thunderstorm outflow and demonstrates the difficulty in comparing thunderstorm and non-thunderstorm winds (Lombardo, Smith *et al.* 2014). The highest mean integral scale values, including a peak of 67.3 m, were noted in the GF2 region for most probes. Excluding the data from Tower 104 yielded only a slight decrease in the mean inflow (outflow) integral scales by 0.5% (1.7%). Similar thunderstorm integral scale results were noted in Orwig and Schroeder (2007) where gust sizes within thunderstorm outflow winds were larger than those of non-thunderstorm winds, despite the use of a different method and a longer averaging time to compute longitudinal integral scales.

The structure of the StickNet array also allowed for the estimation of integral scales based on the cross correlation of towers separated by varying distances. While this method is dependent upon wind direction such that longitudinal integral scales are only captured when the wind direction is parallel to the array, it also allows for the computation of lateral integral scales when the wind direction is perpendicular to the array. Previous research has incorporated this method when the wind direction was  $10 - 30^\circ$  of parallel or perpendicular to the anemometer line for longitudinal and lateral integral scales, respectively (Panofsky 1962, Flay and Stevenson 1988, Hui, Larsen *et al.* 2009). For this event, 40-s segments where the mean wind direction of the fine-scale array (first 5 probes) was within  $20^\circ$  of parallel or perpendicular to the array were used to compute integral length scales. A 50% segment overlap was used to maintain methodological consistency with the autocorrelation results. This threshold and methodology resulted in 24 segments of inflow time periods and five segments of outflow time periods for the computation of longitudinal integral scales, but only one segment when the winds were roughly perpendicular to

the array (during the gust front) for the computation of lateral integral scales. As with the autocorrelation integral scales, an exponential curve was fit to the distance correlation curve (as a function of tower separation) and truncated where the derivative equaled zero. The resulting curve was then integrated to infinity to obtain the integral length scale. For comparison, autocorrelation integral scales were computed as previously described for the segments where the distance correlation method was used.

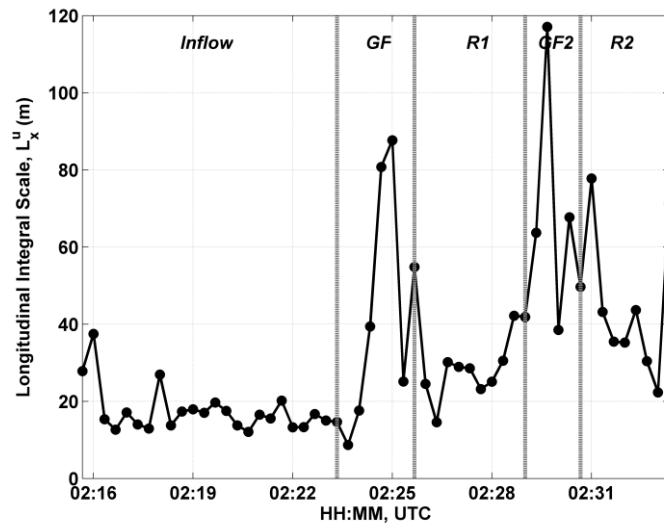


Fig. 10 Time history of the autocorrelation longitudinal integral scale from StickNet Tower 111

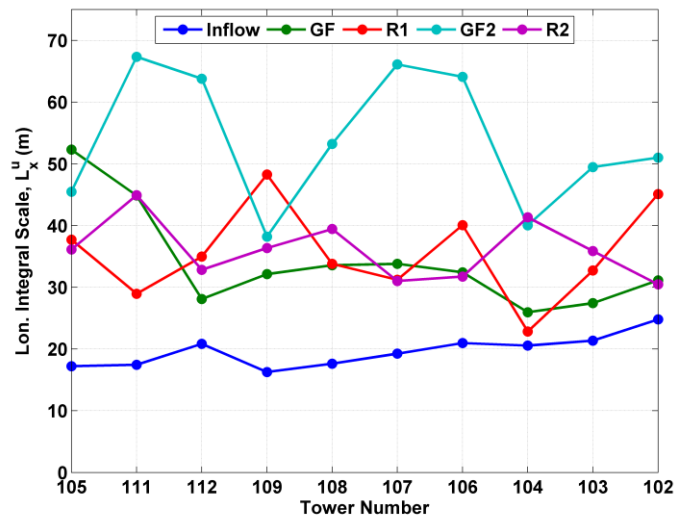


Fig. 11 Spatial distribution of the mean longitudinal integral scales for each outflow region along the array. Towers are arranged west (left) to east (right)

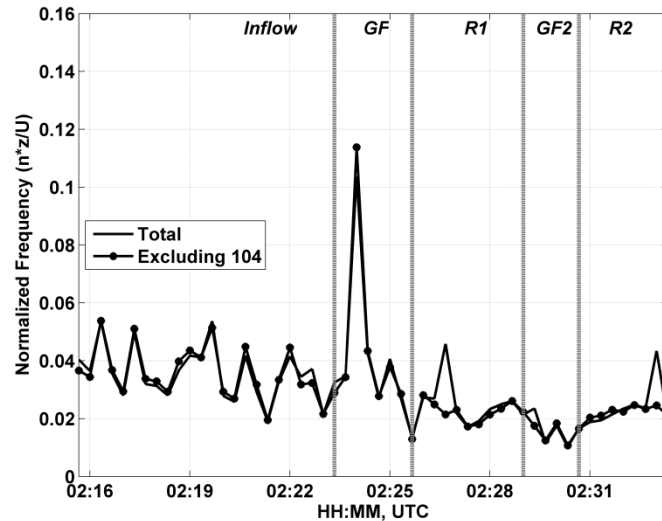


Fig. 12 Time history of peak normalized frequency. The total time history (solid black) represents the mean from all StickNet towers. The time history excluding Tower 104 is also shown with circular markers

The distance correlation method yielded similar results to the autocorrelation method. For the inflow (when the mean wind direction of the fine-scale array was between  $70$  and  $110^\circ$ ), the distance correlation method yielded a mean value of  $20.8$  m. The mean autocorrelation integral scale of the fine scale array for the same 24 segments was computed to be  $20.9$  m. Investigation of the time histories revealed that many of the peaks and troughs were similarly represented by both methods (not shown). Substantially fewer segments were available for the outflow (when the mean wind direction of the fine-scale array was between  $250$  and  $290^\circ$ ), but the trends were similar. The mean integral scale computed with the distance correlation was  $38.6$  m, while the autocorrelation mean was  $39.9$  m. The median values were more divergent but are probably a better estimator of central tendency given the limited number of observations and non-normal distributions. Regardless, the distance correlation method echoes the results of the autocorrelation method in that integral scales, as computed herein, were larger in the outflow of this event.

### 5.3 Spectral analysis

To investigate the distribution of turbulent energy though the course of the event, a short time Fourier Transform (STFT; Cohen 1995) was performed for each 40-s segment and the results compiled into a spectrogram for each tower. In computing the spectrogram, the individual 40-s segments (with the same 50% overlap as the previous section) were first filtered with a 200-point Hanning window. The resulting spectral densities were normalized by variance, and examined in the context of the different regions of the outflow that were previously defined. As interpretation of the spectrograms was complicated by the nonstationary wind speeds within the outflow, the frequency associated with the greatest spectral energy was found in each segment and normalized by the 40-s mean wind speed of the segment to mitigate the influence of the faster wind speeds

(Schroeder and Smith 2003). The resulting time history of the mean peak frequency is shown in Fig. 12 and demonstrates a generally decreasing peak frequency prior to the passage of the gust front. A rapid increase to the maximum peak frequency was observed near the gust front. This maximum was most likely related to the turbulent mixing present at the leading edge of the gust front as the wind speed increases and the wind direction begins to change. After the passage of the gust front, the frequency containing the peak energy continued to decrease, reaching minimum in the GF2 region (Fig. 12). This observation agrees with the longitudinal integral scale analysis which saw the mean eddy size increase up to and eventually peak in the GF2 region and remain elevated (as compared to the inflow) through R2. Additionally, the data from Tower 104 was also removed to isolate the effects of the potentially erroneous wind direction. Several peaks within the R1 and R2 regions were directly attributable to the data from Tower 104.

## 6. Conclusions

High-resolution measurements were collected in a severe thunderstorm complex that produced extensive high-wind reports and wind damage across West Texas. Examination of WSR-88D radar data and WTM data indicated several different features, including a bowing portion of the complex and an embedded circulation, that were verified in the TTUKa mobile Doppler radar data as well as data from TTU StickNet. These different features allowed for the segregation of the 40-s mean wind direction time histories into different regions, such that the effects of features on the 40-s mean wind speed, peak 1-s gusts, and turbulence parameters could be analyzed. The mean wind speeds demonstrated remarkable correlation across the extent of the array, which has implications for the loading of long-span structures such as bridges or transmission lines (Chen and Letchford 2006, Holmes, Hangan *et al.* 2008). Peak 1-s gusts were observed to occur in conjunction with either the circulation or the main body of the outflow, while ramp times to the peak 1-s gust exceed 300 s for all towers. By separating the residual turbulence from the raw time history with a 40-s moving average, running turbulence intensity, integral scales and spectra were computed. Turbulence intensity within the main body of the outflow was comparable to inflow turbulence intensity values, yet reduced in magnitude as compared to other outflow regions. Further, larger scales of turbulence became more active within the GF2 and R2 regions as noted by the increase in longitudinal integral scales and the decrease in normalized peak frequency with time. The synthesis of these observations demonstrates that while turbulence is enhanced at the gust front, the latter is not necessarily the location of the peak wind speeds or wind damage.

The goal of this study was to provide an overview of the event while employing simple, yet effective techniques to examine the turbulence characteristics and compare these characteristics to previous events. While many of the features observed in the Pep, Texas, MCS were specific to the synoptic, mesoscale, and even microscale characteristics driving the event, the quality of the deployment and the magnitude of this event will support further analysis. Of particular interest are the effects of dynamical drivers, such as rear inflow jets and meso-/miso-vortices, on the distribution of peak winds within convective complexes as well as the effects of these features on outflow turbulence characteristics. Future analyses could also incorporate more sophisticated techniques (e.g., Chen and Lechford 2005, Orwig 2010) to further examine the unique evolution of turbulence captured in this dataset. Future data collection efforts will involve even closer tower spacing and refined array configurations to more thoroughly document the lateral scales of turbulence both in thunderstorm and non-thunderstorm environments to investigate hypotheses of

greater lateral correlation in thunderstorm outflow winds and the effect of such correlations on long span structures.

## Acknowledgments

This research is supported by NSF Grant CMMI-1000160. Special thanks to Rich Krupar for his tireless maintenance of the StickNet fleet and leading the StickNet deployment for this event. This work would have not been possible without the help of numerous graduate students and faculty during Project SCOUT.

## References

- American Society of Civil Engineers (ASCE), (2010), "Minimum design loads for buildings and other structures", ASCE/SEI 7-10, Reston, VA.
- Brock, F.V. and Richardson, S.J. (2001), *Meteorological Measurement Systems*, Oxford University Press, New York, United States of America.
- Chen, L. and Letchford, C.W. (2005), "Proper orthogonal decomposition of two vertical profiles of full-scale nonstationary downburst wind speeds", *J. Wind Eng. Ind. Aerod.*, **93**(3), 187-216.
- Chen, L. and Letchford, C.W. (2006), "Multi-scale correlation analyses of two lateral profiles of full-scale downburst wind speeds", *J. Wind Eng. Ind. Aerod.*, **94**(9), 675-696.
- Choi, E.C.C. (2004), "Field measurement and experimental study of wind speed profile during thunderstorms", *J. Wind Eng. Ind. Aerod.*, **92**(3-4), 275 - 290.
- Choi, E.C.C. and Hidayat, F.A. (2002), "Gust factor for thunderstorm and non-thunderstorm winds", *J. Wind Eng. Ind. Aerod.*, **90**(12-15), 1683-1696.
- Cohen, L. (1995), *Time-Frequency Analysis*. Prentice-Hall PTR, New Jersey, United States of America.
- Counihan, J. (1975), "Adiabatic atmospheric boundary layers: a review and analysis of data from the period 1880-1972", *Atmos. Environ.*, **9**(10), 871-905.
- Flay, R.G.J. and Stevenson, D.C. (1988), "Integral length scales in strong winds below 20 m", *J. Wind Eng. Ind. Aerod.*, **28**(1-3), 21-30.
- Fujita, T.T. (1978), "Manual of downburst identification". SMRP Res. Pap. No. 156, Dept. Geophys. Sci., University of Chicago, 104.
- Fujita, T.T. (1981), "Tornadoes and downbursts in the context of generalized planetary scales", *J. Atmos. Sci.*, **38**, 1511-1534.
- Goff, R.C. (1976), "Vertical structure of thunderstorm outflows", *Mon. Weather Rev.*, **104**, 1429-1440.
- Gunter, W.S. and Schroeder, J.L. (2015), "High-resolution full-scale measurements of thunderstorm outflow winds", *J. Wind Eng. Ind. Aerod.*, **138**, 13-26.
- Holmes, J.D. (2001), *Wind Loading of Structures*. Taylor and Francis, New York, United States of America.
- Holmes, J.D., Hangan, H.M., Schroeder, J.L., Letchford, C.W. and Orwig, K.D. (2008), "A forensic study of the Lubbock-Reese downdraft of 2002", *Wind Struct.*, **11**(2), 137-152.
- Hui, M.C.H., Larsen, A. and Xiang, H.F. (2009), "Wind turbulence characteristics study at the Stonecutters Bridge site: Part II: Wind power spectra, integral length scales and coherences", *J. Wind Eng. Ind. Aerod.*, **97**(1), 48-59.
- Kim, J. and Hangan, H. (2007), "Numerical simulations of impinging jets with application to downbursts", *J. Wind Eng. Ind. Aerod.*, **95**(4), 279-298.
- Kwon, D. and Kareem A. (2014), "Revisiting gust averaging time and gust effect factor in ASCE 7", *J. Struct. Eng. - ASCE*, **140**, 06014004-1.

- Letchford, C.W., Mans, C. and Chay, M.T. (2002), "Thunderstorms -- their importance in wind engineering ( a case for the next generation wind tunnel)", *J. Wind Eng. Ind. Aerod.*, **90**(12-15), 1415-1433.
- Lin, W.E., Orf, L.G., Savory, E. and Novacco, C. (2007), "Proposed large-scale modeling of the transient features of a downburst", *Wind Struct.*, **10**(4), 315-346.
- Lombardo, F.T., Smith, D.A., Schroeder, J.L. and Mehta, K.C. (2014), "Thunderstorm characteristics of importance to wind engineering", *J. Wind Eng. Ind. Aerod.*, **125**, 121-132.
- Mason, M.S., Fletcher, D.F and Wood, G.S. (2010), "Numerical simulation of idealised three-dimensional downburst wind fields", *Eng. Struct.*, **32**(11), 3558-3570.
- National Weather Service (NWS) (2013), Significant Weather Events (<http://www.srh.noaa.gov/lub/?n=events-2013-20130605-storms>); Accessed 26 April 2016.
- Orf, L.G., Kantor, E. and Savory E. (2012), "Simulation of a downburst-producing thunderstorm using a very high-resolution three-dimensional cloud model", *J. Wind Eng. Ind. Aerod.*, **104-106**, 547-557.
- Orwig, K.D. (2010), "Examining strong winds from a time-varying perspective", Ph.D. dissertation, Texas Tech University, Lubbock.
- Orwig, K.D. and Schroeder, J.L. (2007), "Near-surface wind characteristics of extreme thunderstorm outflows", *J. Wind Eng. Ind. Aerod.*, **95**(7), 565-584.
- Panofsky, H.A. (1962), "Scale analysis of atmospheric turbulence at 2 m", *Q. J. Roy. Meteor. Soc.*, **88**(375), 57-69.
- Schroeder, J.L. and Smith, D.A. (2003), "Hurricane Bonnie wind flow characteristics as determined from WEMITE", *J. Wind Eng. Ind. Aerod.*, **91**, 767-789.
- Schroeder, J.L., Burgett, W.S., Haynie, K.B., Sonmez, I., Skwira, G.D., Doggett, A.L. and Lipe, J.W. (2005), "The West Texas Mesonet: A technical overview", *J. Atmos. Ocean. Tech.*, **22**, 211-222.
- Simiu, E. and Scanlan, R.H. (1986), "*Wind Effects on Structures*. 2nd ed., Wiley-Interscience, New York, United States of America.
- Skinner, P.S., Weiss, C.C., Schroeder, J.L., Wicker, L.J. and Biggerstaff, M.I. (2011), "Observations of the surface boundary structure within the 23 May 2007 Perryton, Texas, supercell", *Mon. Weather Rev.*, **139**, 3730-3749.
- Storm Prediction Center (SPC) (2013), Storm Reports. [http://www.spc.noaa.gov/climo/reports/130605\\_rpts.html](http://www.spc.noaa.gov/climo/reports/130605_rpts.html). Accessed 26 April 2016.
- Stull, R.B. (1988), "*An Introduction to Boundary Layer Meteorology*", Vol. 13. Springer Science & Business Media.
- Teunissen, H.W. (1980), "Structure of mean winds and turbulence in the planetary boundary layer over rural terrain", *Bound. - Lay. Meteorol.*, **19**(2), 187-221.
- Vermeire, B.C., Orf, L.G. and Savory, E. (2011), "Improved modeling of downburst outflows for wind engineering applications using a cooling source approach", *J. Wind Eng. Ind. Aerod.*, **99**(8), 801-814.
- Wakimoto, R.M. (1982), "The life cycle of thunderstorm gust fronts as viewed with Doppler radar and rawinsonde data", *Mon. Weather Rev.*, **110**, 1060-1082.
- Wakimoto, R.M., Murphey, H.V., Davis, C.A. and Atkins, N.T. (2006), "High winds generated by bow echoes. Part II: The relationship between the mesovortices and damaging straight-line winds", *Mon. Weather Rev.*, **134**, 2813-2829.
- Weiss, C.C. and Schroeder, J.L. (2008), "StickNet: A new portable rapidly deployable surface observations system", *Bull. Amer. Meteor. Soc.*, **89**, 1502-1503.
- Wood, G.S., Kwok, K.C.W., Motteram, N.A. and Fletcher, D.F. (2001), "Physical and numerical modeling of thunderstorm downbursts", *J. Wind Eng. Ind. Aerod.*, **89**(6), 535-552.